ARTICLES
https://doi.org/10.1038/s41563-018-0144-z
nature materials

# Robust microscale superlubricity in graphite/hexagonal boron nitride layered heterojunctions

Yiming Song[1,2], Davide Mandelli[3], Oded Hod[3], Michael Urbakh[3], Ming Ma[1,2]* and Quanshui Zheng[2,4]*

**Structural superlubricity is a fascinating tribological phenomenon, in which the lateral interactions between two incommensurate contacting surfaces are effectively cancelled resulting in ultralow sliding friction. Here we report the experimental realization of robust superlubricity in microscale monocrystalline heterojunctions, which constitutes an important step towards the macroscopic scale-up of superlubricity. The results for interfaces between graphite and hexagonal boron nitride clearly demonstrate that structural superlubricity persists even when the aligned contact sustains external loads under ambient conditions. The observed frictional anisotropy in the heterojunctions is found to be orders of magnitude smaller than that measured for their homogeneous counterparts. Atomistic simulations reveal that the underlying frictional mechanisms in the two cases originate from completely different dynamical regimes. Our results are expected to be of a general nature and should be applicable to other van der Waals heterostructures.**

Friction and wear are the two central causes for energy loss and component failure in mechanical systems[1]. Traditional friction reduction approaches often involve liquid lubricants that may fail under strong confinement and extreme external conditions, such as high loads and temperatures, as well as in the presence of chemical contamination or under a vacuum environment. Structural superlubricity may provide a viable alternative route to the reduction of friction and wear that relies on the effective cancellation of lateral forces within incommensurate rigid crystalline contacts[2–10]. Originally observed in nanoscale homogeneous graphitic contacts more than a decade ago[6], in recent years several independent experimental efforts have demonstrated its successful scale-up to the micrometre regime[7,10–16]. A major obstacle standing against the widespread application of structural superlubricity involves the strong anisotropic nature of friction in homogeneous rigid interfaces with respect to their relative orientation. Even when placed in an incommensurate ultralow friction configuration they exhibit a tendency to rotate towards the aligned commensurate configuration during the sliding motion and eventually lock in a high friction state[17]. The severity of this problem grows with contact size due to the increasing frictional anisotropy.

As a possible remedy, one may consider the formation of multicontact junctions that include rigid polycrystalline surfaces of randomly oriented patches, which prevent the formation of extended commensurate interfaces. This, however, introduces numerous domain walls that may cause pinning effects and result in the enhancement of friction. To resolve this problem, a recent realization of the multicontact approach used a graphene-coated corrugated sphere that slides atop flat graphite or hexagonal boron nitride (hBN) surfaces[14]. The surface corrugation led to the formation of merely a few separated contact points between the sphere and the flat substrate. As a result, superlubric motion was obtained for both the homogeneous and heterogeneous interfaces. Nevertheless, the application of large normal loads on such a small contact area results in extremely high local pressures that may eventually lead to enhanced wear, and thus reduce the system durability. To avoid this, it has been suggested that heterogeneous junctions of extended single-crystalline surfaces provide structural superlubricity that is robust against crystal reorientations and exhibits enhanced durability[18,19]. Here, due to the intrinsic lattice constant mismatch of the contacting surfaces, incommensurability also exists in the aligned configuration, in which the lattice vectors of the two surfaces are parallel.

As a significant understanding of the tribological properties of rigid layered graphitic contacts has been gained over the past decade, a natural platform to examine structural superlubricity in heterojunctions is the interface between graphite and its inorganic hBN counterpart. In the present study, we address this challenge by constructing pristine microscale junctions between single-crystalline graphite and hBN and measure their tribological properties. We find that the orientational anisotropy of friction in the heterogeneous junction is orders of magnitude lower than that of the corresponding homogeneous graphitic interface. Therefore, ultralow friction is preserved even for the aligned contact, which makes the system extremely robust against dynamic reorientation processes. This also holds true under ambient conditions and normal loads as high as 100 μN, which, for our contact area of ~9 μm$^2$, corresponds to a pressure of ~11 MPa. Using fully atomistic molecular dynamics simulations we further reveal that the origin of frictional anisotropy in homo- and heterojunctions is governed by completely different physical mechanisms and frictional regimes.

To demonstrate the robustness of superlubricity in heterojunctions we used an atomic force microscope (AFM) manipulator (Fig. 1 and Methods give further details as to the experimental set-up) to measure the dependence of the friction force on the relative angular orientation between the graphite and hBN surfaces (Fig. 2). During these measurements the sliding velocity and normal load were kept constant at 200 nm s$^{-1}$ and 19.7 μN, respectively.

[1]State Key Laboratory of Tribology, Department of Mechanical Engineering, Tsinghua University, Beijing, China. [2]Center for Nano and Micro Mechanics, Tsinghua University, Beijing, China. [3]Department of Physical Chemistry, School of Chemistry, The Raymond and Beverly Sackler Faculty of Exact Sciences and The Sackler Center for Computational Molecular and Materials Science, Tel Aviv University, Tel Aviv, Israel. [4]Department of Engineering Mechanics, Tsinghua University, Beijing, China. *e-mail: maming16@tsinghua.edu.cn; zhengqs@tsinghua.edu.cn

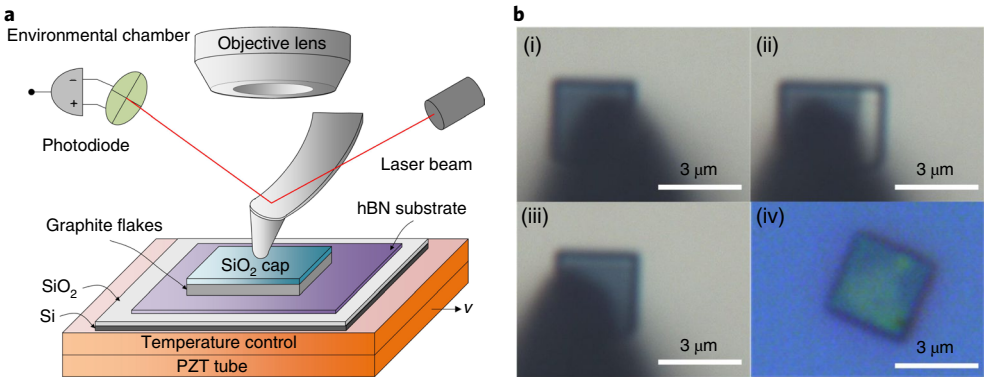


**Fig. 1 | Experimental set-up. a**, Schematic diagram of the experimental set-up to measure the friction in graphite/hBN junctions. An hBN substrate was rigidly fixed to the AFM stage on top of which a $SiO_2$ capped graphitic flake was placed. The stage consisted of a piezoelectric ceramic transducer (PZT), a heater band and a Si/$SiO_2$ surface. Normal and lateral forces were applied via an AFM probe put in contact with the central area of the $SiO_2$ cap. An objective lens was coupled to the AFM head to follow the relative movement of the sheared flake with respect to the hBN substrate in situ. **b**, Optical images of the fabrication process of the graphite/hBN heterostructure. Attachment of a tungsten probe to the $SiO_2$ cap of an HOPG mesa (i). Tungsten probe shearing of a graphitic mesa results in the drag of the mesa's top section (ii). Self-retraction motion exhibited by the dragged graphitic flake atop the lower graphite mesa section on release from the tungsten probe (iii). Transfer of the graphitic flake onto the hBN surface (iv).

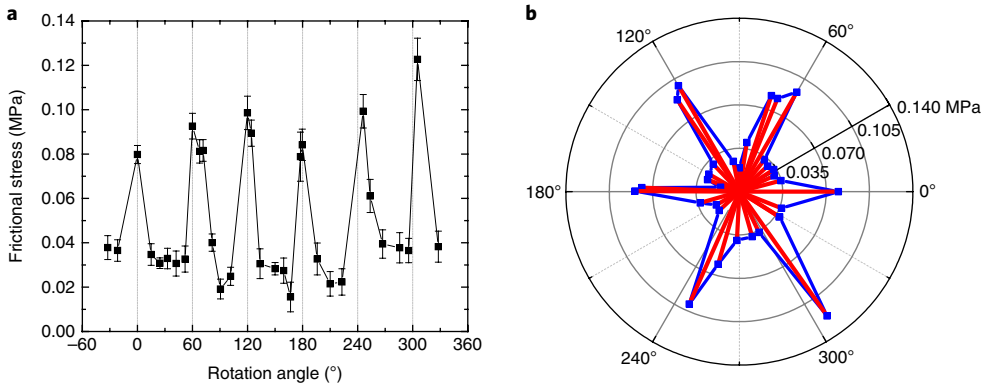


**Fig. 2 | Rotational anisotropy of the measured friction of a graphite/hBN heterojunction.** Dependence of the frictional stress on the relative interfacial orientation between monocrystalline graphite and hBN measured under ambient conditions (temperature of 22 ± 1 °C and relative humidity of 29 ± 3%). The sliding velocity was set to 200 nm $s^{-1}$ and the normal load was kept at 19.7 μN. **a**,**b**, Both linear (**a**) and polar (**b**) representations of the data are provided to demonstrate clearly the anisotropy and six-fold symmetry of the measured friction. The estimated accuracy of the reported rotation angles is ±0.5°. To increase the angular resolution requires a significant increase of the experimental duration that would, in turn, lead to enhanced instrumental drift effects and thus decrease the signal-to-noise ratio. The corresponding frictional stress error bars in **a** represent the standard deviation of the results obtained from 16 independent frictional measurements. Supplementary Section 3 gives further details of the error estimation.

The measured friction force exhibits a six-fold symmetry, which clearly shows the hexagonal nature of the underlying lattices, and further indicates the monocrystallinity of the contacting surfaces[18]. The typical friction force obtained for the rotationally misaligned contact is ~300 nN. When divided by the contact area of 9 $μm^2$, this translates into a frictional stress of merely ~0.03 MPa, comparable to the value of 0.01 MPa measured in 0.2 $μm^2$ misaligned homogeneous graphitic contacts[10]. Notably, although the microscale homogeneous graphitic contacts lock in when placed at the aligned configuration, which renders them impossible to shear with our apparatus, the heterogeneous contact exhibits only a small anisotropy with less than a fourfold enhancement of friction. The strong anisotropy found for the former can be readily understood in terms of a rotational transition from a misaligned incommensurate interface that exhibits smooth sliding to a commensurate aligned contact, characterized by pronounced stick–slip motion. More surprising is the anisotropy observed in the heterojunction case. Here, even for the aligned contact, the interface remains incommensurate due to the intrinsic lattice vector misfit of the two surfaces. Hence, in this case, one would expect smooth sliding to occur regardless of the interfacial misorientation angle, which leads to negligible orientational frictional anisotropy[18,19].

To unravel the physical origin of the orientational frictional anisotropy in homogeneous and heterogeneous contacts and the differences between the underlying mechanisms, we invoked fully atomistic molecular dynamics simulations[19–22]. Our model system consisted of a flexible graphene layer dragged atop a rigid hBN or graphene layer via a stage that was modelled as a rigid flat duplicate of the graphene layer, as schematically shown in Fig. 3a. Each atom within the graphene layer was connected via a harmonic spring to its image atom within the stage. The interaction between the graphene layer and the underlying hBN or graphene substrates was modelled with the graphene/hBN or Kolmogorov–Crespi interlayer potentials (ILPs)[21,23], respectively, whereas the intralayer interactions within the graphene layer were modelled using the reactive bond order (REBO) potential (the Methods section gives further details)[24]. The validity of the rigid substrate approximation was confirmed by performing test simulations that involved mobile multilayered hBN substrates (Supplementary Section 8 gives further details).

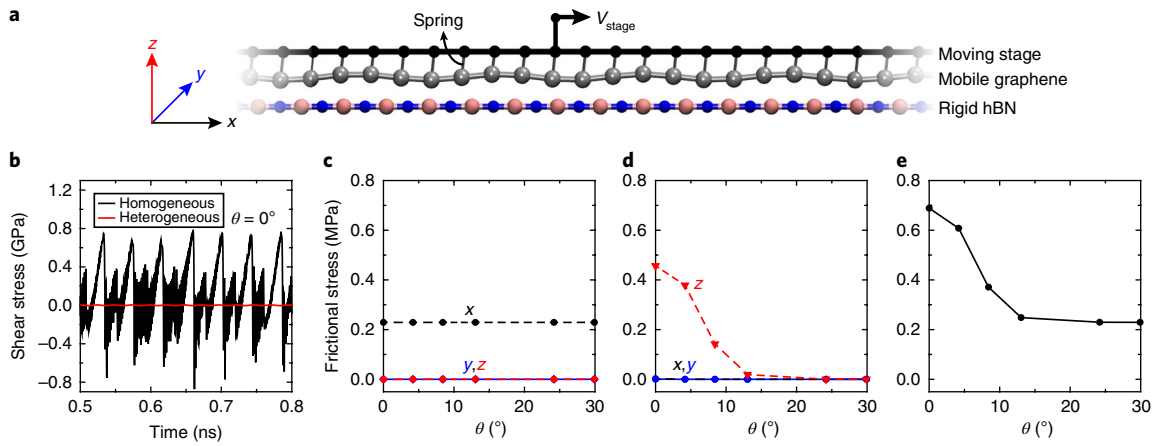


**Fig. 3 | Simulated rotational anisotropy of the friction of a graphite/hBN heterojunction. a**, Schematics of the simulation set-up. A fully mobile graphene layer is dragged over a rigid hBN substrate monolayer by a stage that moves at a constant velocity, $v_{stage}$. The stage is modelled by a rigid duplicate of the mobile graphene layer, each atom of which is connected to its image within the stage model via harmonic springs. Normal load, not considered herein, can be applied by exerting a vertical force to each atom of the slider. Periodic boundary conditions are implemented in the lateral directions. **b**, Simulated friction traces in the aligned ($\theta = 0°$) heterogeneous graphene/hBN junction (red line) compared to the homogeneous graphene/graphene counterpart (black line); **c**,**d**, Angular dependence of the contributions to the overall frictional stress from the graphene COM motion (**c**) and from the internal degrees-of-freedom (motion of the slider atoms with respect to its COM) (**d**) as defined in equation (2). Contributions that correspond to the lateral motion parallel and perpendicular to the sliding direction (see reference frame in **a**) are represented by black and blue lines, respectively. Red lines represent the contribution along the vertical direction. **e**, Angular dependence of the overall (sum over all components) frictional stress calculated for the heterogeneous graphene/hBN junction. All the results presented here were obtained using uniform stage/graphene spring constants of $K = 11$ meV Å$^{-2}$ and a driving velocity of $v_{stage} = 10$ m s$^{-1}$. The damping coefficients are chosen as $\eta_z = 4.425$ ps$^{-1}$ and $\eta_x = \eta_y = 0.029$ ps$^{-1}$. These values reproduce well the experimental frictional anisotropy and give the correct shear stress values at the experimental sliding velocity assuming a logarithmic scaling. The Methods section gives more details on the methodology and simulation parameters.

In our simulations, the overall frictional stress, $\tau$, that develops during the sliding motion can be written as a sum of the contributions of the different degrees of freedom (DOF) within the graphene layer to the energy dissipation as follows[25]:

$$\tau = \frac{m_C}{S v_{stage}} \left[ N \sum_{\alpha=x,y,z} \eta_\alpha v_{COM,\alpha}^2 + \sum_{\alpha=x,y,z} \eta_\alpha \sum_{i=1}^{N} \left\langle (v_{i,\alpha} - v_{COM,\alpha})^2 \right\rangle \right] \quad (1)$$

where $v_{i,\alpha}$ and $v_{COM,\alpha}$ are the instantaneous velocity components of carbon atom $i$ and of the centre-of-mass (COM) of the entire graphene layer along the $\alpha$ direction, respectively, $m_C$ is the mass of a carbon atom, $N$ is the number of carbon atoms within the graphene layer, $S$ is the overall contact area; $v_{stage}$ is the drag velocity of the stage, $\eta_\alpha$ is the damping coefficient that characterizes the kinetic energy dissipation rate along the $\alpha$ direction and $\langle\ \rangle$ denotes a steady-state time average. The parameter values used in our simulations are given in the caption of Fig. 3.

For the homogeneous graphene junction, we found that the overall frictional stress, calculated from equation (2) is dominated by energy dissipation through the COM DOF. Specifically, for the aligned homogeneous case, a total frictional stress of 135 MPa was obtained due to the highly dissipative COM stick–slip motion (Fig. 3b, black curve). For the 30° misaligned graphitic contact, a smooth sliding was obtained and the calculated frictional stress dropped to 0.23 MPa, which resulted in a significant kinetic friction anisotropy factor of ~600 (Supplementary Section 6). An even larger drop was found for the static friction, which reduced from ~800 MPa for the aligned contact to vanishingly small values (<60 kPa) on a 30° rotation away from alignment. These results correspond well with previous observations of frictional anisotropy in nanoscale graphitic contacts[6] and with our present experimental findings that a complete junction lock in occurs at the aligned configuration versus the superlubric motion measured for the misaligned graphitic contact.

The experimental observation of a significantly smaller frictional anisotropy in the heterogeneous graphite/hBN junctions suggests a completely different underlying dynamic mechanism. This is clearly demonstrated by our simulations, which show that the energy dissipation through the DOF of the COM is more than three orders of magnitude smaller than that obtained for the aligned homogeneous junction and is independent of the misalignment angle (Fig. 3c). This can be attributed to the smooth soliton-like motion of the moiré pattern ridges that characterize the heterogeneous junction, which eliminates the COM stick–slip instability[19], as shown by the red curve in Fig. 3b. Therefore, consideration of the COM motion alone cannot explain the observed frictional anisotropy[18,19]. As a consequence, the internal DOF become the dominant factor that dictates the frictional behaviour in these systems. As can be clearly seen in Fig. 3d, the out-of-plane motion of the carbon atoms provides the main energy dissipation route. As the out-of-plane distortions in these systems are strongly influenced by the moiré superstructure (Supplementary Section 9 gives a detailed description of the moiré superstructures), they rapidly decay with increasing interfacial misfit angle[21,26,27]. Therefore, this channel of energy dissipation demonstrates a significant anisotropy of three orders of magnitude. Finally, when the COM and internal DOF contributions are combined, the heterogeneous junction exhibits ultralow friction for all misfit angles with a small anisotropy, similar to that measured in the experiment (Fig. 3e). The overall frictional stress anisotropy factor obtained in the simulation depends on the ratio between the in-plane ($\eta_{x,y}$) and out-of-plane ($\eta_z$) damping coefficients, as in equation (2). Notably, previous studies predicted that the damping coefficient in the normal direction can be orders of magnitude larger than the lateral values[28,29]. In particular, for carbon atoms adsorbed on graphite, the ratio, $\eta_{x,y}/\eta_z$, equals ~0.006

(see Methods section). As there is no rigorous estimation of the values of damping coefficients that should be used for graphene flakes that slide on hBN, we tuned the ratio between the damping coefficients in lateral and normal directions to reproduce the fourfold anisotropy of the frictional stress observed experimentally. Interestingly, for our model bilayer heterojunction this is achieved for $\eta_{x,y}/\eta_z \approx 0.007$, which is close to the theoretical estimation mentioned above (an evaluation of the sensitivity of the frictional anisotropy to the number of substrate layers is reported in Supplementary Section 8). The absolute values of $\eta_x = \eta_y = 0.029\,\mathrm{ps}^{-1}$ and $\eta_z = 4.425\,\mathrm{ps}^{-1}$ were chosen to reproduce the order of magnitude of the measured shear stress at the experimental sliding velocities ($10^2$–$10^4\,\mathrm{nm\,s}^{-1}$, much smaller than the simulated value of $v_{\mathrm{stage}} = 10\,\mathrm{m\,s}^{-1}$), after accounting for the observed logarithmic scaling (see below). The final values fall in the range typically adopted in molecular dynamics simulations of nanoscale friction[30], and are close to theoretical estimations of damping coefficients for adsorbed atoms[31].

We note that recent simulations using an empirically parameterized ILP indicated the existence of a rotational anisotropy of the energy dissipation within graphene/hBN junctions[32]. The use of our recently developed graphene/hBN ILP, which was carefully parameterized against state-of-the-art first-principles reference data, enabled us to obtain a quantitative understanding of this phenomenon and allowed for a direct comparison with the experimental observations (Supplementary Section 11 gives further details).

As dynamical structural superlubricity is not a critical phenomenon, a common definition for achieving a superlubric state is given such that the kinetic friction coefficient, defined as the local derivative of the friction force with respect to the applied normal load, should be below $10^{-3}$. To estimate the kinetic friction coefficient obtained in our system, we present in Fig. 4a the normal load dependence of the frictional stress measured for misaligned contacts at various sliding velocities. Under ambient conditions, the kinetic frictional stress was found to be nearly independent of the normal load up to the highest measured value of 100 μN (black squares in Fig. 4a), regardless of the sliding velocity, yielding a negligible kinetic friction coefficient smaller than $1.4\times10^{-4}$, well within the superlubric regime. The frictional stress was also found to be mostly independent of the normal load for the aligned interface (Supplementary Section 1), which results in friction coefficients smaller than $5.9\times10^{-3}$. We note that recent microscale ball-on-surface experiments demonstrated friction coefficients as low as $2.5\times10^{-3}$ in multicontact graphene/hBN heterojunctions[14]. Furthermore, macroscale superlubricity with friction coefficients of $4\times10^{-3}$ were obtained in diamond-like-carbon/graphene-scroll junctions[33]. Our planar monocrystalline atomically smooth interface allows us to obtain friction coefficients that are at least an order of magnitude lower than these.

Notably, we found that during the sliding process the graphitic mesas tend to persist either in the higher or lower friction states, which correspond to the aligned and misaligned interface configurations, respectively (6 out of 22 higher friction measurements resulted in rotation towards the low friction state and 4 out of 38 lower friction measurements resulted in rotation towards the higher friction state). This is in contrast to the case of homogeneous graphitic junctions, in which the large anisotropy renders the low friction state to be dynamically unstable and leads to lock in of the system in the high-friction state. Our findings are in line with recent experimental observations that reported two stable configurations of graphene on hBN that corresponded to the aligned and 30° rotated ~0.2 μm² interfaces[34].

An important factor that needs to be taken into account in every frictional measurement is the effect of environmental conditions, specifically the influence of surface contaminants on the measured friction. Therefore, to evaluate the intrinsic frictional contribution of the heterogeneous interface, we repeated the measurements under an inert nitrogen environment using several 150 °C thermally annealed junctions (the Methods section gives details on the thermal annealing procedure). After annealing, the frictional stress that resulted remained practically load independent and reduced by nearly a factor of two (typical results are presented by the green diamonds in Fig. 4a), which suggests that in this case about half of the friction measured under ambient conditions results from surface contaminants.

The extremely low frictional stresses reported above under ambient conditions are alone appealing for energy loss reduction purposes. However, another factor that is essential for practical

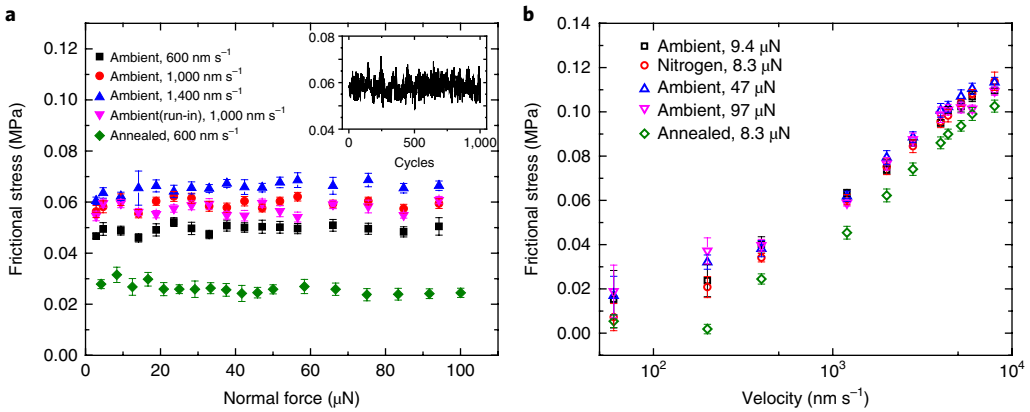


**Fig. 4 | Effects of external conditions on the friction of misaligned graphite/hBN interfaces. a**, Load dependence of the frictional stress between monocrystalline graphite and hBN surfaces measured at various sliding velocities, which ranged from 600 to 1,400 nm s$^{-1}$. Measurements performed under ambient conditions are compared to the results from a sample that was 150 °C pre-annealed and measured under nitrogen atmosphere (green diamonds). The run-in process of 1,000 friction loops (~2 mm in total (inset)) was performed at a normal load of 47 μN and a speed of 1 μm s$^{-1}$ under ambient conditions. **b**, Dependence of the measured frictional stress on the sliding velocity at various normal loads, which ranged from 8.3 to 97 μN. Measurements performed under ambient conditions are compared to the results of a sample that was 150 °C pre-annealed and measured under a nitrogen atmosphere (green diamonds). All the presented frictional stresses were obtained by averaging over 16 scan loops with an overall distance of 64 μm. The frictional stress error bars represent the standard deviation of the results obtained from 16 independent frictional measurements. Supplementary Section 3 gives further details regarding the error estimation.

applications is system durability. To evaluate the durability of the heterojunction we subjected one of the samples to repeated frictional cycles for up to 1,000 loops with an overall travelled distance of ~2 mm at a speed of 1 μm $s^{-1}$ while applying a normal load of 47 μN. The inset of Fig. 4a reports the friction force as a function of cycle number and shows no significant drift. Following this, we repeated the load dependence frictional measurement, reported in the ambient (run-in) data set (magenta symbols) of Fig. 4a. These results clearly demonstrate that the system behaviour was not affected by the run-in procedure and thus indicating that the accumulation of mechanical wear is effectively hindered in our system by the superlubric motion.

Finally, another key factor for realistic tribological scenarios is the ability to achieve superlubricity at high sliding velocities. To this end, we measured the dependence of the frictional stress on the sliding velocity up to 10 μm $s^{-1}$ at a temperature of 25 °C under ambient conditions (relative humidity of 42%) as well as under a nitrogen atmosphere (relative humidity <10%) with and without pre-annealing at 150 °C. As demonstrated in Fig. 4b a relatively slow logarithmic increase of the frictional stress with the sliding velocity was obtained for all the samples studied, in agreement with the theory of thermally activated friction processes[30]. Consistent with Fig. 4a, no appreciable dependence on the normal load was observed. The friction under ambient conditions and under a nitrogen environment without annealing is practically the same, which indicates the minor role that humidity plays in the present set-up. Furthermore, both are consistently larger than the friction obtained for the pre-annealed sample (green diamond), which demonstrates yet again the effectiveness of thermal annealing for cleaning edge and surface contaminants.

In summary, an experimental realization of structural superlubricity in microscale heterogeneous contacts between monocrystalline graphite and hBN, which is robust against crystal reorientations, was demonstrated. The orientational anisotropy of the sliding friction was found to be orders of magnitude smaller than that of the corresponding homogeneous graphitic contact. We rationalized these results via fully atomistic molecular dynamics simulations that reveal completely different physical mechanisms of frictional anisotropy. For the homogeneous graphitic junction, it is dominated by dissipation through the COM motion, whereas in the heterojunction it originates mainly from the internal DOF of the contacting layers. Specifically, in the aligned configuration the latter exhibits enhanced out-of-plane atomic undulations that are related to the soliton-like moiré superstructure motion[19]. These undulations rapidly decay upon rotation to an orientationally misaligned configuration, in which the sliding surface remains flat.

Interestingly, a related mechanism for frictional anisotropy was demonstrated previously for a completely different system that included a two-dimensional (2D) array of colloidal particles sliding over an incommensurate optical lattice[35]. This indicates that robust structural superlubricity is a phenomenon of a general nature, which, with proper design, is expected to be attainable not only in 2D layered material interfaces but also in other dry rigid contacts as well as in soft-matter systems.

With the aim to scale up such results towards mesoscopic and macroscopic contacts, one should consider junctions that include lattice defects and polycrystalline surfaces. Lattice defects may include vacancies and Stone–Wales bond rotations[36], which reduce interfacial commensurability. In this respect, they are expected to lower the overall friction[37]. Furthermore, when using polycrystalline junctions, different surface regions are randomly oriented and thus the frictional stress is expected to become completely independent of the interlayer misalignment angle. Nevertheless, the effects of grain boundary and defect-induced pinning on the overall friction remains to be investigated.

## Methods

Methods, including statements of data availability and any associated accession codes and references, are available at https://doi.org/10.1038/s41563-018-0144-z.

Received: 4 August 2017; Accepted: 2 July 2018;
Published online: 30 July 2018

## References

1. Holmberg, K., Andersson, P. & Erdemir, A. Global energy consumption due to friction in passenger cars. *Tribol. Int.* **47**, 221–234 (2012).
2. Hirano, M. & Shinjo, K. Atomistic locking and friction. *Phys. Rev. B* **41**, 11837–11851 (1990).
3. Hirano, M. & Shinjo, K. Superlubricity and frictional anisotropy. *Wear* **168**, 121–125 (1993).
4. Shinjo, K. & Hirano, M. Dynamics of friction—superlubric state. *Surf. Sci.* **283**, 473–478 (1993).
5. Martin, J. M., Donnet, C., Lemogne, T. & Epicier, T. Superlubricity of molybdenum disulfide. *Phys. Rev. B* **48**, 10583–10586 (1993).
6. Dienwiebel, M. et al. Superlubricity of graphite. *Phys. Rev. Lett.* **92**, 126101 (2004).
7. Liu, Z. et al. Observation of microscale superlubricity in graphite. *Phys. Rev. Lett.* **108**, 205503 (2012).
8. Yang, J. et al. Observation of high-speed microscale superlubricity in graphite. *Phys. Rev. Lett.* **110**, 255504 (2013).
9. Kawai, S. et al. Superlubricity of graphene nanoribbons on gold surfaces. *Science* **351**, 957–961 (2016).
10. Koren, E., Lörtscher, E., Rawlings, C., Knoll, A. W. & Duerig, U. Adhesion and friction in mesoscopic graphite contacts. *Science* **348**, 679–683 (2015).
11. Zhang, R. et al. Superlubricity in centimetres-long double-walled carbon nanotubes under ambient conditions. *Nat. Nanotech.* **8**, 912–916 (2013).
12. Liu, Y., Grey, F. & Zheng, Q. The high-speed sliding friction of graphene and novel routes to persistent superlubricity. *Sci. Rep.* **4**, 4875 (2014).
13. Vu, C. C. et al. Observation of normal-force-independent superlubricity in mesoscopic graphite contacts. *Phys. Rev. B* **94**, 081405(R) (2016).
14. Liu, S. W. et al. Robust microscale superlubricity under high contact pressure enabled by graphene-coated microsphere. *Nat. Commun.* **8**, 14029 (2017).
15. Li, H. et al. Superlubricity between $MoS_2$ monolayers. *Adv. Mater.* **29**, 1701474 (2017).
16. Sheehan, P. E. & Lieber, C. M. Friction between van der Waals solids during lattice directed sliding. *Nano Lett.* **17**, 4116–4121 (2017).
17. Filippov, A. E., Dienwiebel, M., Frenken, J. W. M., Klafter, J. & Urbakh, M. Torque and twist against superlubricity. *Phys. Rev. Lett.* **100**, 046102 (2008).
18. Leven, I., Krepel, D., Shemesh, O. & Hod, O. Robust superlubricity in graphene/*h*-BN heterojunctions. *J. Phys. Chem. Lett.* **4**, 115–120 (2013).
19. Mandelli, D., Leven, I., Hod, O. & Urbakh, M. Sliding friction of graphene/hexagonal-boron nitride heterojunctions: a route to robust superlubricity. *Sci. Rep.* **7**, 10851 (2017).
20. Leven, I., Azuri, I., Kronik, L. & Hod, O. Inter-layer potential for hexagonal boron nitride. *J. Chem. Phys.* **140**, 104106 (2014).
21. Leven, I., Maaravi, T., Azuri, I., Kronik, L. & Hod, O. Interlayer potential for graphene/*h*-BN heterostructures. *J. Chem. Theor. Comput.* **12**, 2896–2905 (2016).
22. Maaravi, T., Leven, I., Azuri, I., Kronik, L. & Hod, O. Interlayer potential for homogeneous graphene and hexagonal boron nitride systems: reparametrization for many-body dispersion effects. *J. Phys. Chem. C* **121**, 22826–22835 (2017).
23. Kolmogorov, A. N. & Crespi, V. H. Registry-Dependent Interlayer Potential for Graphitic Systems. *Phys. Rev. B* **71**, 235415 (2005).
24. Donald, W. B. et al. A second-generation reactive empirical bond order (REBO) potential energy expression for hydrocarbons. *J. Phys. Cond. Matt* **14**, 783–802 (2002).
25. Weiss, M. & Elmer, F.-J. Dry friction in the Frenkel–Kontorova–Tomlinson model: dynamical properties. *Z. Phys. B Cond. Mat.* **104**, 55–69 (1997).
26. Woods, C. R. et al. Commensurate–incommensurate transition in graphene on hexagonal boron nitride. *Nat. Phys.* **10**, 451–456 (2014).
27. van Wijk, M. M., Schuring, A., Katsnelson, M. I. & Fasolino, A. Moiré Patterns as a probe of interplanar interactions for graphene on h-BN. *Phys. Rev. Lett.* **113**, 135504 (2014).
28. Persson, B. N. J. & Ryberg, R. Brownian motion and vibrational phase relaxation at surfaces: CO on Ni(111). *Phys. Rev. B* **32**, 3586–3596 (1985).
29. Persson, B. N. J., Tosatti, E., Fuhrmann, D., Witte, G. & Woll, C. Low-frequency adsorbate vibrational relaxation and sliding friction. *Phys. Rev. B* **59**, 11777–11791 (1999).
30. Vanossi, A., Manini, N., Urbakh, M., Zapperi, S. & Tosatti, E. Colloquium: modeling friction: from nanoscale to mesoscale. *Rev. Mod. Phys.* **85**, 529–552 (2013).

31. Persson B. N. J. *Sliding Friction: Physical Principles and Applications* (Springer, Berlin, 1998).
32. Guerra, R., van Wijk, M., Vanossi, A., Fasolino, A. & Tosatti, E. Graphene on *h*-BN: to align or not to align? *Nanoscale* **9**, 8799–8804 (2017).
33. Berman, D., Deshmukh, S. A., Sankaranarayanan, S. K., Erdemir, A. & Sumant, A. V. Friction. Macroscale superlubricity enabled by graphene nanoscroll formation. *Science* **348**, 1118–1122 (2015).
34. Wang, D. et al. Thermally induced graphene rotation on hexagonal boron nitride. *Phys. Rev. Lett.* **116**, 126101 (2016).
35. Mandelli, D., Vanossi, A., Manini, N. & Tosatti, E. Friction boosted by equilibrium misalignment of incommensurate two-dimensional colloid monolayers. *Phys. Rev. Lett.* **114**, 108302 (2015).
36. Stone, A. J. & Wales, D. J. Theoretical studies of icosahedral $C_{60}$ and some related species. *Chem. Phys. Lett.* **128**, 501–503 (1986).
37. Braiman, Y., Hentschel, H. G. E., Family, F., Mak, C. & Krim, J. Tuning friction with noise and disorder. *Phys. Rev. E* **59**, R4737–R4740 (1999).


## Acknowledgements

Q.Z. acknowledges the financial support from the NSFC (Grant no. 11572173), the National Basic Research Program of China (Grant no. 2013CB934200), the SRFDP (Grant no. 20130002110043) and the Cyrus Tang Foundation. M.M. acknowledges the financial support from the Thousand Young Talents Program (Grant no. 61050200116) and the NSFC (Grant no. 11632009 and 11772168). Y.M.S. and M.M. thank L. Ge from the NT-MDT Beijing Office and P. Cheng from Oxford Instruments China for their help in experimental device support. O.H. is grateful for financial support of the Israel Science Foundation under Grant no. 1586/17, the Lise Meitner Minerva Center for Computational Quantum Chemistry, the Center for Nanoscience and Nanotechnology at Tel Aviv University, and the Naomi Foundation via the 2017 Kadar Award. M.U. acknowledges financial support from the Deutsche Forschungsgemeinschaft, Grant no. BA 1008/21-2, and the COST Action MP1303. D.M. acknowledges the fellowship from the Sackler Center for Computational Molecular and Materials Science at Tel Aviv University, and from the Tel Aviv University Center for Nanoscience and Nanotechnology.

## Author contributions

M.M., O.H., M.U. and Q.Z. conceived the original idea behind this study. M.M. and Q.Z. designed the experimental aspects of the study, Y.S. performed the experiments and Y.S. and M.M. analysed the experimental data with contributions from all the authors. D.M., O.H. and M.U. designed and analysed the simulations. D.M. wrote the code and conducted the simulations. All authors contributed to the writing of this manuscript.

## Competing interests

The authors declare no competing interests.

## Additional information

**Supplementary information** is available for this paper at https://doi.org/10.1038/s41563-018-0144-z.

**Reprints and permissions information** is available at www.nature.com/reprints.

**Correspondence and requests for materials** should be addressed to M.M. or Q.Z.

**Publisher's note:** Springer Nature remains neutral with regard to jurisdictional claims in published maps and institutional affiliations.

## Methods

**Preparation of hBN substrate.** High-quality hBN (Momentive Materials) crystals were mechanically exfoliated by the Scotch tape method[38] and transferred onto a silicon substrate with a $SiO_2$ layer of ~300 nm in thickness. For measurements performed without an annealing stage, the silicon substrate was mechanically attached to the scanner of the AFM apparatus using a metallic clamp. For measurements performed with an annealing stage, the silicon substrate was attached to a heater band by heat-conducting glue, and then the heater band was magnetically attached to the scanner of the AFM apparatus. No relative motion between the silicon substrate and the scanner of the AFM apparatus was observed during all the experiments.

**Graphite flake preparation.** Square graphitic mesas of lateral and vertical dimensions of $3\times3\,\mu m^2$ and about 1 μm, respectively, were lithographically fabricated on highly ordered pyrolitic graphite (HOPG, ZYB grade (Brucker))[39]. The mesas were capped with a 400 nm thick $SiO_2$ layer, to which a tungsten microtip controlled by a micromanipulator (Kleindiek MM3A) was attached. Graphitic flakes were prepared by applying a shear stress onto the HOPG mesas[8,13,40,41] using the micromanipulator until they split along their vertical direction; the lower section remained rigidly attached to the substrate and the upper graphitic stack was dragged by the microtip. To assure that the contacting graphene layer is chemically clean and monocrystalline, we chose only flakes that exhibited self-retraction motion (in two orthogonal directions) as validated by optical microscopy (HiRox KH-3000) (Fig. 1)[7].

**Surface characterization.** The quality of the contacting hBN and graphite surfaces was validated using an AFM apparatus and Raman spectroscopy. First, the roughness of the hBN substrate was measured using an Asylum Research MFP-3D Infinity AFM in tapping mode with the aim to identify extended smooth regions (<0.4 nm in roughness (Supplementary Fig. 4a)) and with lateral dimensions of at least $8\times8\,\mu m^2$ to be used in the friction measurements (Supplementary Fig. 4a). To verify the monocrystallinity of the chosen region, the crystal lattice orientation of nine $10\times10\,nm^2$ spots was measured using the Asylum Research Cypher S AFM apparatus (Supplementary Fig. 4c). The crystalline lattice orientation of all nine spots was found to be identical (within our instrumental uncertainty related to the sample/tip drift), which thus strongly indicates the monocrystallinity of the target hBN substrate region.

The contacting surface of the transferred graphitic flake could not be directly characterized because it was facing down and thus hidden from our measuring instruments (yellow surface in Supplementary Fig. 5a). Nevertheless, to evaluate its quality, we investigated the counterpart upper surface of the graphitic mesa, from which the flake was cleaved (red surface in Supplementary Fig. 5a). Similar to the hBN substrate, the crystal structure of nine $10\times10\,nm^2$ spots, equally distributed across the $3\times3\,\mu m^2$ graphitic surface, were characterized using an Asylum Research Cypher S AFM (Supplementary Fig. 5b,c). Here, as well, our high-resolution images (Supplementary Fig. 5d) demonstrate an identical lattice orientation for all nine spots, which indicates that the upper mesa surface (and hence also the down-facing contacting surface of the flake) is, indeed, monocrystalline in accordance with previous studies on similar systems[7,8,41]. This conclusion is further supported by the observed 60° rotational symmetry of the frictional stress measured for the graphite/hBN heterojunction (Fig. 2).

To characterize further the degree of crystallinity of the graphitic surface, we conducted Raman spectroscopy measurements of the upper surface of the cleaved graphitic mesa. As the area of the Raman laser spot is roughly a ninth of the entire mesa surface area, by scanning over all nine spots marked in blue in Supplementary Fig. 5b we nearly covered the entire mesa top. The Raman spectra obtained by measuring over all nine spots are superimposed in Supplementary Fig. 6. The absence of the characteristic D peak at 1,350 $cm^{-1}$ in all the measured spectra clearly demonstrates that the surface is nearly pristine. This is further validated by the 2D map in Supplementary Fig. 7, which presents the spatially resolved ratio between the D and G Raman peak intensities ($I_D/I_G$) of the top surface of the cleaved graphite mesa. The square blue region, which corresponds to low $I_D/I_G$ ratio, that covers almost the entire surface indicates the nearly complete absence of defects.

**Graphite/hBN heterojunctions formation.** The selected graphitic flakes were transferred to the preselected atomically smooth region of the hBN substrate using the microtip and micromanipulator (Fig. 1).

**Friction measurements.** The frictional measurements of the graphene/hBN heterostructures were performed under an ambient atmosphere (temperature of $22\pm1$ °C and relative humidity of $29\pm3$%). The experimental set-up included a commercial NTEGRA upright AFM (NT-MDT), a 100 μm XYZ piezoelectric tube scanner, a high numerical aperture objective lens (×100 (Mitutoyu)) equipped with a top visual AFM probe (VIT-P tip (NT-MDT)) and a heating stage (SU045NTF (NT-MDT)) that reached a maximal temperature of 150 °C. Figure 1a shows a schematic representation of the set-up. The AFM tip was within the field of view of the optical microscope when it was in contact with the $SiO_2$ cap of the graphitic mesas. The AFM tip was calibrated in situ by the Sader method[42,43] for the normal direction and the wedge calibration method[44] for the lateral direction.

Prior to the friction-force measurements, the contacts were cleaned by applying several hundred shear loops (each of 2 μm in length) until the measured shear stresses reached a steady state. This process was shown to remove surface contaminants located outside the contacting area due to wiping effect in the direction of sliding[45], as well as intercalated contaminants confined within the interface that experience enhanced diffusion[46]. Once steady state was achieved, the friction force was evaluated as the average energy (averaged over 16 loops) dissipated during a steady-state shear-force loop divided by the overall cycle length. The relative angular orientation between the graphite and hBN surfaces was controlled via AFM tip manipulation of the graphite flake, and a scan direction perpendicular to the AFM's cantilever was adopted throughout the friction measurements. The external normal load was controlled through a feedback loop of the scan electronics.

To enable a relatively large contact area between the tip (whose original radius was ~10 nm) and the $SiO_2$ cap of the graphite mesa, prior to the friction measurements a relatively large normal force of ~100 μN, was intentionally applied to induce a plastic deformation of the tip. The scanning electron microscope image of the deformed tip shown in Supplementary Fig. 9a clearly demonstrates the flattening of the tip and increase of its contact radius to ~0.5 μm. Compared to the $3\times3\,\mu m^2$ surface area of the graphite slider, this suggests that some pressure gradient may still develop across the frictional interface. Nevertheless, one should consider the multilayer nature of the slider and the silicon oxide cap that comes in contact with the tip. These may serve as buffer layers that spread the load more evenly across the interface (see Supplementary section 5 for a detailed analysis of this effect).

**Atmosphere control.** To stabilize the local environment near the sample, all the friction measurements were performed in a homemade 7 litre seamless aluminium chamber. A rubber ring was used to seal the interface between the chamber and the AFM substrate. Prior to each experimental realization performed under nitrogen protection (with or without annealing), the chamber was flushed with nitrogen gas at a flow rate of 2 litre $min^{-1}$ for a period of 70 min.

**Thermal annealing.** As detailed in the main text, in some of the experimental realizations a thermal annealing pretreatment was applied. To this end, after the nitrogen-flushing stage the temperature of the heater band was increased from room temperature to 150 °C within 6 min, upon reaching this temperature it was kept constant for half an hour and then allowed to cool back to room temperature for about 2 h. The friction measurements with the annealed samples were performed under a nitrogen environment as detailed above.

**Computational system description.** Infinite, twisted graphene/hBN interfaces were modelled by means of commensurate periodic supercells generated using a published method[47]. Given the primitive lattice vectors $\mathbf{b}_1=a_{hBN}(1,0)$, $\mathbf{b}_2=a_{hBN}(1/2,\sqrt{3}/2)$, $\mathbf{g}_1=a_g(\cos\theta,\sin\theta)$, $\mathbf{g}_2=a_g(1/2\cos\theta-\sqrt{3}/2\sin\theta,1/2\sin\theta+\sqrt{3}/2\cos\theta)$ of hBN and graphene (rotated by angle $\theta$), respectively, a commensurate supercell can be constructed for each set of four integers $\{n_1,n_2,m_1,m_2\}$ that satisfy the condition $n_1\mathbf{g}_1+n_2\mathbf{g}_2=m_1\mathbf{b}_1+m_2\mathbf{b}_2$. The resulting supercell corresponds to a triangular lattice of periodicity $L=|n_1\mathbf{g}_1+n_2\mathbf{g}_2|$ that contains $N_g=n_1^2+n_1n_2+n_2^2$, and $N_{hBN}=m_1^2+m_1m_2+m_2^2$ primitive cells of graphene and hBN, respectively. In practice, we fixed the lattice constant of graphene to the equilibrium value of the adopted REBO potential, $a_g=a_{REBO}=2.42106$ Å, and searched for different sets $\{n_1,n_2,m_1,m_2,\theta\}$ with the constraint that the ratio between the lattice constant of hBN ($a_{hBN}$) and that of graphene, $\rho=a_{hBN}/a_g$ should be close to the experimental lattice mismatch $\rho_{exp}\approx1.0183$ (ref. [26]). A similar procedure was used to generate commensurate supercells for twisted graphene/graphene interfaces. In Supplementary Section 12 we report the parameters used to construct the various heterogeneous and homogeneous commensurate supercells discussed.

**Simulation set-up.** In our simulation set-up, which aimed to mimic the friction-force experiments, a graphene monolayer is dragged along a rigid graphene or hBN substrate. Unlike previous studies that were based either on purely geometric considerations[18] or quasi-static calculations[19], here we performed fully dynamic simulations that solved Langevin's equations of motion for all dynamic particles in the system. This was found to be essential to capture the frictional orientational anisotropy observed experimentally. The pulling apparatus was represented by a rigid duplicate of the dragged monolayer positioned parallel to the underlying surface, whose COM was displaced along the substrate to represent the experimental moving stage. Normal loads were modelled by applying a homogeneous constant force to each atom of the mobile slider. In fact, loads typically used in the presented experimental results ($\lesssim10^{-4}$ nN $atom^{-1}$) are, for all practical purposes, very small and therefore we mainly performed simulations at zero normal load. Tests performed at a load of $10^{-4}$ nN $atom^{-1}$ gave quantitatively similar results. We note that relaxing the assumption of a rigid substrate is expected to increase the calculated frictional stress at small misfit angles, $\theta\lesssim5°$ with a minor effect at larger angles. Consequently, the calculated orientational frictional stress anisotropy may become somewhat larger, but still within good agreement with the experimental observations.

The in-plane interactions between the rigid duplicate and the sliding graphene monolayer were described by classical harmonic springs that connect each graphene atom with its counterpart on the rigid duplicate. The presented results were obtained for a spring constant of $K_{\|} = 11$ meV Å$^{-2}$ in the lateral $(x,y)$ directions for all graphene atoms. This value corresponds to the equilibrium curvature of the Kolmogorov–Crespi[23] potential for lateral displacements at the equilibrium interlayer distance of a graphene bilayer. The interlayer interactions between the sliding monolayer and the substrate were described by the Kolmogorov–Crespi potential and the graphene/hBN ILP[21] for graphene and hBN substrates, respectively. The intralayer interactions within the dragged graphene monolayer were described using the second generation REBO potential[24]. The corresponding equilibrium carbon–carbon distance was 1.3978 Å, which yielded a lattice constant of 2.421 Å. This value was used to construct the graphene monolayer, whereas for hBN we chose a lattice constant that approximately gave the experimental 1.8% intralayer lattice mismatch for the heterojunction (Supplementary Table 1). This methodology was shown to reproduce accurately the potential energy surface for the two interfaces considered here[21,48]. We note that the ILP was designed to augment intralayer terms. To this end, each atom was assigned a layer identifier such that the interactions between atoms residing in the same layer were described by the intralayer term, whereas the interactions between atoms residing in different layers were described by the interlayer term.

The large $3\times3$ μm$^2$ microscale contact studied suggests that surface contributions to kinetic friction dominate over possible edge effects, and therefore we considered infinite homogeneous graphene/graphene and heterogeneous graphene/hBN interfaces. To study the angular anisotropy of friction, we built appropriate supercells that corresponded to different misalignment angles between the crystallographic axes of the sliding graphene monolayer and that of the substrate following a published method[47] and briefly outlined above. In all the simulations, periodic boundary conditions (PBC) were implemented in the lateral directions. Hence, all contacts considered here were, strictly speaking, commensurate. Nevertheless, static friction-force simulations for the twisted homogeneous junction and for all heterogeneous contacts resulted in vanishingly small values. This indicates that our commensurate supercells also faithfully represent their incommensurate counterparts. We further checked that the model systems adopted are at convergence with respect to finite size effects, as discussed in Supplementary Section 10. Our supercell models are therefore also expected to represent well infinite and truly incommensurate interfaces.

**Simulation protocol.** For each misalignment angle, we first performed a full geometry relaxation of the sliding monolayer using the FIRE algorithm[49]. The relaxation procedure was terminated when the forces that act on each degree of freedom reduced below $10^{-6}$ eV Å$^{-1}$. Starting from the fully relaxed configurations, sliding simulations were performed by moving the rigid duplicate at a constant velocity $v_{\mathrm{stage}}$ of 10 m s$^{-1}$ along the zigzag direction of the substrate, which corresponds to the $x$ axis of our Cartesian frame of reference. The instantaneous shear stress was evaluated as the sum of the forces that act on the stage atoms in the driving direction. The kinetic frictional stress was calculated by time averaging the shear stress at steady-state sliding. The static friction force was measured by applying an increasing homogeneous external force in the $x$ direction to all carbon atoms and monitoring by the COM displacement of the graphene layer. During this protocol, the external force was incremented in steps of $\Delta F = 10^{-6}$ eV Å$^{-1}$. In practice, all the incommensurate contacts considered were already free to slide at the smallest applied force $F = \Delta F$.

All simulations results presented were obtained by solving the following equations of motion (which imply zero temperature, $T = 0$ K) for all carbon atoms of the graphene slider:

$$m_C\ddot{\mathbf{r}}_i = -\nabla_{\mathbf{r}_i}(V_{\mathrm{inter}}^{\mathrm{ILP}} + V_{\mathrm{intra}}^{\mathrm{REBO}}) + K_{\|}(\mathbf{r}_{\|,i}^{\mathrm{stage}} - \mathbf{r}_{\|,i}) + F_i^{\mathrm{damp}} \quad (2)$$

The first and second terms in the right-hand side of equation (2) are the forces due to the inter- and intralayer interactions, respectively, and the third term is the elastic driving acting in the $(x,y)$ plane. To mimic the energy dissipation, we introduced viscous forces that act directly on each atom of the dragged monolayer:

$$F_i^{\mathrm{damp}} = -m_C \sum_{\alpha=x,y,z} \eta_\alpha v_{\alpha,i}\hat{\boldsymbol{\alpha}} \quad (3)$$

Here $\hat{\boldsymbol{\alpha}}$ is a unit vector along direction $a = x,y,z$, $v_{\alpha,i}$ is the velocity component of atom $i$ along the $\alpha$ direction and $\eta_\alpha$ is the corresponding damping coefficient required to reach a steady-state motion[30]. We qualitatively estimated the anisotropy of the damping coefficients based on a theory of the damping of lateral and normal oscillations of surface adsorbates[28], which predicts a fourth-power dependence of the damping coefficients on the harmonic oscillation frequency $\eta_\alpha \propto \omega_\alpha^4$. We computed $\omega_\alpha$ from the parallel and perpendicular oscillation frequencies of a single carbon atom over graphene around its equilibrium position, giving $\omega_{x,y} \cong 19.6098$ THz, $\omega_z \cong 70.5520$ THz and $\eta_{x,y}/\eta_z = (\omega_{x,y}/\omega_z)^4 \approx 0.006$. We note here that the frequency dependence of the damping coefficient may be different for mono- or multilayer configurations. For the case of a commensurate adsorbed monolayer, a square dependence of $\eta_\alpha \propto \omega_\alpha^2$ was previously predicted[29]. As a theoretical evaluation of the scaling has not yet been provided for the incommensurate case of interest to us, we decided to estimate the damping coefficient anisotropy based on the single-adsorbate model.

To investigate the effects of finite temperature, we also performed Langevin dynamics simulations at $T > 0$, by including in equation (2) a random force that satisfies the fluctuation–dissipation theorem. In summary, thermal effects were found to have only a minor influence on the calculated frictional stress. A detailed discussion of the results and of the protocol adopted in these simulations is reported in Supplementary Section 7.

**Evaluation of frictional dissipation.** In our simulations, the instantaneous shear force is given by the sum of the lateral spring forces, $F_{\mathrm{i}}(t) = K_{\|}(\mathbf{r}_{\|,i}^{\mathrm{stage}} - \mathbf{r}_{\|,i})$, that act between the atoms of the sliding graphene layer and those of its rigid duplicate within the moving stage. The kinetic friction force, $F_{\mathrm{k}}$, is evaluated as the total shear force that acts on the moving stage in the sliding direction, $F_{\mathrm{k}} = \left\langle \sum_{i=1}^{N_{\mathrm{p}}} F_{i,x}(t) \right\rangle$, where $N_{\mathrm{p}}$ is the number of driven atoms and $\langle\ \rangle$ denotes a steady-state time average. The time average is taken after the initial transient dynamics decays and the system reaches steady-state motion that corresponds to a balance between the (time-averaged) power $P_{\mathrm{in}}$ generated by the external springs:

$$P_{\mathrm{in}} = \sum_{i=1}^{N_{\mathrm{p}}} \langle \mathbf{F}_i(t) \cdot \mathbf{v}_i(t) \rangle = F_{\mathrm{k}} v_{\mathrm{stage}} \quad (4)$$

and the power $P_{\mathrm{out}}$ dissipated by the internal viscous forces:

$$\begin{aligned} P_{\mathrm{out}} &= \sum_{i=1}^{N_{\mathrm{p}}} m_i \sum_{\alpha=x,y,z} [\eta_\alpha \langle (v_{i,\alpha}(t))^2 \rangle] \\ &= \sum_{i=1}^{N_{\mathrm{p}}} m_i \sum_{\alpha=x,y,z} [\eta_\alpha \langle (v_{i,\alpha}(t) - v_{\mathrm{COM},\alpha}(t))^2 \rangle] \\ &+ M_{\mathrm{tot}} \sum_{\alpha=x,y,z} \eta_\alpha \langle (v_{\mathrm{COM},\alpha}(t))^2 \rangle \end{aligned} \quad (5)$$

Equation (5) demonstrates that the frictional dissipation can be divided into COM motion contributions in the lateral and perpendicular directions and the corresponding terms related to the kinetic energy dissipated via the internal DOF of the graphene layer. Careful analysis of the various terms allowed us to explain the differences in the frictional behaviour of the homogeneous and heterogeneous junctions in terms of the nature of the dominating dissipative channels and revealed the underlying frictional mechanisms.

**Data availability.** The data that support the findings of this study are available from the corresponding authors upon reasonable request.

## References


38. Lee, C. et al. Frictional characteristics of atomically thin sheets. *Science* **328**, 76–80 (2010).
39. Lu, X. K., Yu, M. F., Huang, H. & Ruoff, R. S. Tailoring graphite with the goal of achieving single sheets. *Nanotechnology* **10**, 269–272 (1999).
40. Wang, W. et al. Measurement of the cleavage energy of graphite. *Nat. Commun.* **6**, 7853 (2015).
41. Zheng, Q. et al. Self-retracting motion of graphite microflakes. *Phys. Rev. Lett.* **100**, 067205 (2008).
42. Sader, J. E., Larson, I., Mulvaney, P. & White, L. R. Method for the calibration of atomic force microscope cantilevers. *Rev. Sci. Instrum.* **66**, 3789–3798 (1995).
43. Sader, J. E., Chon, J. W. M. & Mulvaney, P. Calibration of rectangular atomic force microscope cantilevers. *Rev. Sci. Instrum.* **70**, 3967–3969 (1999).
44. Ogletree, D. F., Carpick, R. W. & Salmeron, M. Calibration of frictional forces in atomic force microscopy. *Rev. Sci. Instrum.* **67**, 3298–3306 (1996).
45. Liu, Z. et al. A graphite nanoeraser. *Nanotechnology* **22**, 265706 (2011).
46. Ma, M. et al. Diffusion through bifurcations in oscillating nano- and microscale contacts: fundamentals and applications. *Phys. Rev. X* **5**, 031020 (2015).
47. Trambly de Laissardiere, G., Mayou, D. & Magaud, L. Localization of Dirac electrons in rotated graphene bilayers. *Nano Lett.* **10**, 804–808 (2010).
48. Reguzzoni, M., Fasolino, A., Molinari, E. & Righi, M. C. Potential energy surface for graphene on graphene: ab initio derivation, analytical description, and microscopic interpretation. *Phys. Rev. B* **86**, 245434 (2012).
49. Bitzek, E., Koskinen, P., Gähler, F., Moseler, M. & Gumbsch, P. Structural relaxation made simple. *Phys. Rev. Lett.* **97**, 170201 (2006).